The use of non-vacuum electron beam (NVEB) technology as an universal manufacturing process for welding and cutting of high-strength steels

IOP Conf. Series: Journal of Physics: Conf. Series **1089** (2018) 012012 doi:10.1088/1742-6596/1089/1/012012

The use of non-vacuum electron beam (NVEB) technology as an universal manufacturing process for welding and cutting of high-strength steels

A Beniyash, G Klimov and T Hassel

Institute of Materials Science, Leibniz Universität Hannover, Germany

e-mail: beniyash@iw.uni-hannover.de

Abstract. This publication presents the advantages of NVEB technology as an universal tool for material processing based on our investigations on welding and cutting of high-strength S960QL, S1100 and S1300 steels. In this work, the effect of welding cooling time $t_{8/5}$ on the microstructure of the heat-affected zone (HAZ) and mechanical properties of the joints were investigated. The new process NVEB-cutting with a local suction produces extremely high cutting speeds, up to 17 m/min with high quality edges, render this method a significant development for new NVEB-applications. To demonstrate the capabilities of the non-vacuum electron beam as a universal tool for the technological process chain, the samples of steel S1100QL were made, while cutting and welding was carried out by one machine basement. The experimental results will be shown and discussed.

1. Introduction

In the last 20 years, constructors became considerably interested in high-strength steel in different stages of heat treatment with minimum yield strength up to 1300 MPa. These materials are designed primarily for highly loaded welded structures: crane booms and outriggers, shock absorbers, load bearing elements of special importance in modern building constructions [1]. To reduce the influence of welding on the mechanical properties of such steels, a precision control of heat input by the welding is needed. Some publications were devoted to the welding of high-strength steels by arc technologies [2, 3]. S. Blaha and al. reported on experiments with electron beam welding of high-strength steels S960 and Weldox 1300 [4]. In the case of welding S960QL, satisfactory mechanical properties were achieved. These samples failed on the base material and had a bending angle of 180°. In the case of steels Weldox 1100 and Weldox 1300, the ultimate strength R_m reached the level of base Material but the samples failed in the heat-affected zone. The welding process with an electron beam under atmospheric conditions is known as Non-Vacuum Electron Beam Welding (NVEBW). It meets the above mentioned requirements and the investigation of the implementation of this technology for welding of high-strength steels is of great practical interest.

Due to its concentrated and precise energy input, very high welding speed and absence of vacuum chamber NVEBW offers several technological and economic advantages. Non-vacuum electron beam technologies not only have been used for welding processes but recently the Institute of Materials Science of the Leibniz Universität Hannover has developed a versatile and high-speed cutting process for this tool [5, 6]. This means that the EB- machine can be simultaneously used for both processes - cutting and welding [7]. Welded joints characteristics concerning strength, hardness, plasticity and

toughness related to the weld and HAZ (heat affected zone) should diverge from the analogous properties of the base material as little as possible. The most important factors of the welding process influencing the mechanical properties are the preheat temperature, the line energy as well as the work piece thickness and the seam geometry. These factors are summarized in the cooling time $t_{8/5}$ together, which characterized structure transformation within the range of 800° C to 500° C. The cooling time $t_{8/5}$ should be held in the optimum range. Too fast cooling of the welds has an unfavorable effect on the deformation behavior of the connection and hydrogen content in the weld seam. The risk of cold cracks also exists. Too slow cooling of the weld beads from the austenitic temperature field has the consequence that the strength properties of the weld metal do not correspond to those of the base material figure 1.

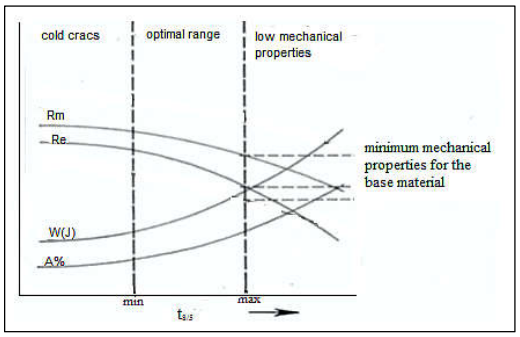

Figure 1. Mechanical properties of a welded joint vs. time $t_{8/5}$, according [8].

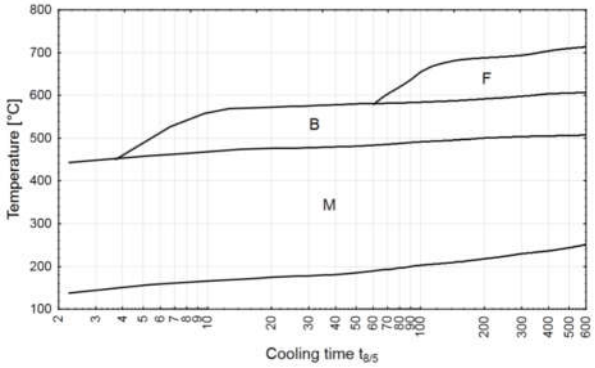

Figure 2. Exemplary CCT-W diagram for Weldox 1300 steel, F – ferrite, B – bainite, M – martensite [3].

The CCT diagrams for welding conditions are used to forecast the structure and to assess the HAZ hardening susceptibility as well as to aid in the design of welding technologies (linear energy and preheating temperature) enabling the obtainment of joints characterized by good plasticity and ductility, protecting the above named area against brittle cracking. The diagram shows the phase relationship within the range of 800° C to 500° C as a function of the cooling time. An exemplary CCT diagram for welding conditions related to steel Weldox 1300 with marked structural areas in the function of cooling time $t_{8/5}$ is presented in figure 2.

Usually the evaluation of the influence of the welding thermal cycle on the material is performed by the implementation of metallographic analysis, which indicates the change in the microstructure. Recently, computer programs have appeared that allow one to evaluate the effect of the thermal welding cycle on the properties of the seam. One such program is a program WeldCalc from SSAB that help the user to optimize the welding parameters [9]. This program was used within the framework of these investigations.

The NVEB cutting (NVEBC) process developed at the Leibniz Universität Hannover is considerably different from standard thermal melt cutting processes. Instead of utilizing a gas jet from a nozzle above the process zone (e.g. plasma cutting) or the direct sublimation of the material (e.g. laser cutting), NVEBC employs a local low vacuum from underneath. The pressure difference across the process zone from atmospheric conditions at the top of the plate and low vacuum at the bottom induces a flow of gas across the melt front that removes the molten material in a highly efficient manner out of the cutting kerf. Moreover, further production steps such as welding and various methods of heat treatment can be performed with the electron beam due to the accurate control of the beam power. In the presented paper the effect of welding thermal cycles of NVEBW properties and microstructure of high strength steels was investigated.

2. Experimental

The experiments were performed on a NVEB welder PTR NV EBW 25-175 TU (PTR Präzisionstechnik GmbH; Germany). The system works with an accelerating voltage of 175 kV and a beam power of up to 25 kW (figure 3). The 3D CNC control system allows linear movements of travel speed up to 20 m/min in *x*, *y* and *z* direction. Non-vacuum electron beam welding employs essentially the same equipment as vacuum electron beam welding except that the working chamber is replaced by an orifice system. The electron beam emerges from the gun column via a series of differentially pumped vacuum stages, which are separated by small diameter orifice nozzles. Thus, the need for evacuation time is eliminated, as the orifice system and the generator column are permanently kept under vacuum. The electron beam is guided to the atmosphere from the high vacuum (10^{-4} mbar) in the electron beam generator over a low vacuum (10^{-2} mbar) and rough vacuum (<1 mbar), see figure 4.

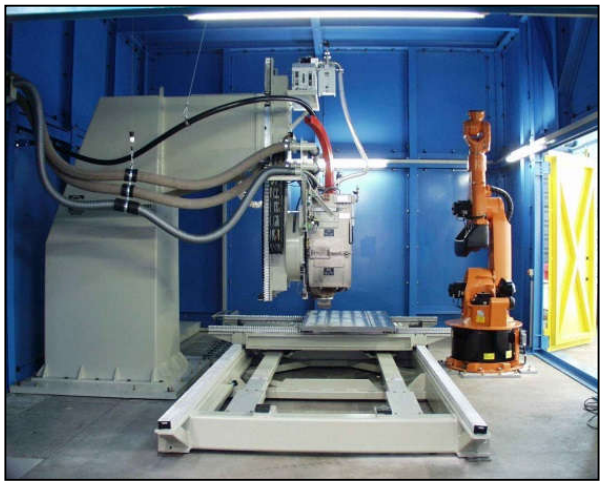

Figure 3. NVEB welder PTR NV EBW 25-175 TU [10].

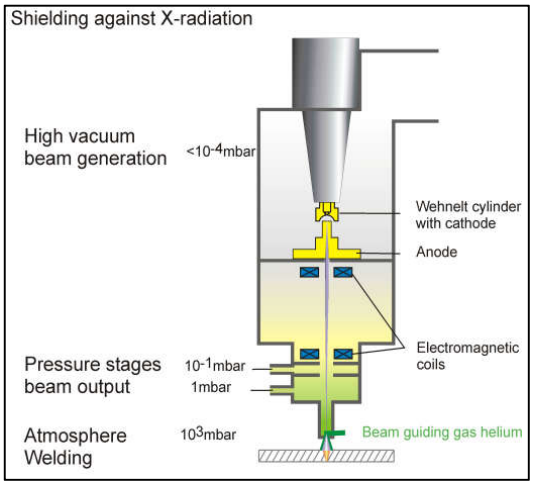

Figure 4. NVEB principal setup.

3. Welding procedure

For welding experiments high strength water quenched steel plates of SSAB steel S960QL S1100 and S1300 6, 8 and 12 mm thickness without preheat were used. The steels are supplied in the heat-treated condition and have a bainitic-martensitic microstructure. The nominal mechanical properties and chemical composition of steels are given in Tables 1 and 2.

Table 1. Mechanical properties of investigated steels [11].

Brand	Re (MPa)	Rm (MPa)	A_5 (%)	Impact energy, J		
				0°	-20°	-40°
Strenx 960QL	850–960	980–1150	10–12	–	–	40
Strenx1100	1100	1250–1550	8–10	–	–	27
Strenx 1300	1300	1400–1700	8	–	27	27

Table 2. Chemical composition of investigated steel [11].

Brand	Chemical composition [%] wt.									
	C_{max}	Si_{max}	Mn_{max}	P_{max}	S_{max}	Cr_{max}	Cu_{max}	Ni_{max}	Mo_{max}	B_{max}
S960QL	0.22	0.86	1.80	0.025	0.012	1.60	0.55	2.10	0.74	0.006
S1100	0.21	0.50	1.40	0.020	0.005	0.80	0.30	3.00	0.70	0.005
S1300	0.25	0.50	1.40	0.020	0.005	0.80	0.30	3.00	0.70	0.005

The experiments were carried out without edge preparation. Some welds were performed in two passes. The second pass served to compensate the welding gaps and form a smooth transition to the base metal. As a filler material, a solid wire Union X90 and a Autrod 12.58 in diameter of 1.2 mm were used. The cooling time $t_{8/5}$ was calculated in WeldCalc 2.2 from SSAB.

Table 3. NVEBW process parameters.

№	Material	Thickn (mm)	Ib (mA)	Working distance (mm)	Welding speed (m/min)	Wire speed (m/min)	Filler material	$t_{8/5}$ (s)	Remarks
1	S960QL	6.5	115	15	3	3	Union X90	–	–
2	S960QL	10	140	10	2.2	–	–	–	–
3	S960Ql	10	50	10	1.4	3	Autrod 12.58	–	cosmetic pass
4	S1100	6.5	–	–	–	–	–	–	–
5	S1100	8	120	15	2.35	–	–	3	–
6	S1300	8	100	12	3.5	–	–	1.3	–
7	S1300	12	120	12	3.5	–	–	1.9	–

4. Mechanical tests

Static tensile tests were carried out according to standard DIN EN10002. The results of mechanical properties of the EBW joint are collected in Table 4.

Table 4. The mechanical properties of the NVEBW joints.

Material	Thickness (mm)	R_e (MPa)	R_m (MPa)	A (%)	Failure area	Impact energy J(-40°)
S960QL	6.5	1037	1190	6.5	Base metal	45.9–57.0
S1100	6.5	1250	1310	2.1	HAZ	50.1–59.0
S1300	6.5	1281	1418	2.5	HAZ	51.9–59.2

Except the specimens made of S960QL steel which failed on base metal, all specimens failed in the HAZ.

The Vickers microhardness HV1 measurements across the HAZ and base metal were carried out on the metallographic samples. The hardness measurements are presented in figures 5, 6 and 7. For the steel S960QL an increase of micro hardness HV1 by 50 units in the weld seam relative to base material was observed, which indicates the presence of a martensitic structure. The hardness of steels S1100 and S1300 showed a micro hardness HV1 of weld seam on the level of base material. All samples showed decrease in the micro hardness in the HAZ. The decreasing a micro hardness HV1 in the HAZ was 70 units for S960QL, 100 units for S1100, and 130 units for S1300, which corresponds to the grade of tempering of the steels.

Metallographic examination revealed that the concentrated electron beam significantly affects the changes of microstructure in the weld and the adjacent heat affected zone (HAZ). The fundamental differences in the microstructure of three examined steels were not observed. The three zones, depending on the distance from the weld face, can be distinguished on figure 8.

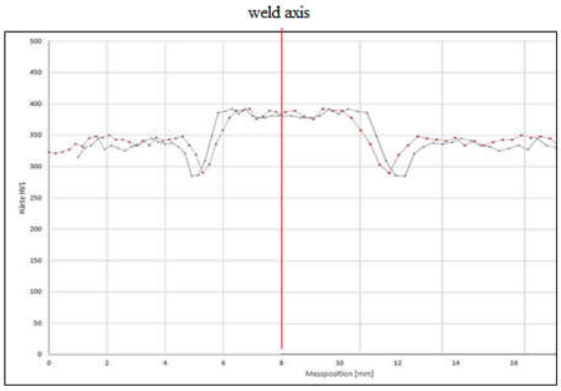

Figure 5. HV1 hardness of welded joints made of steel 960QL.

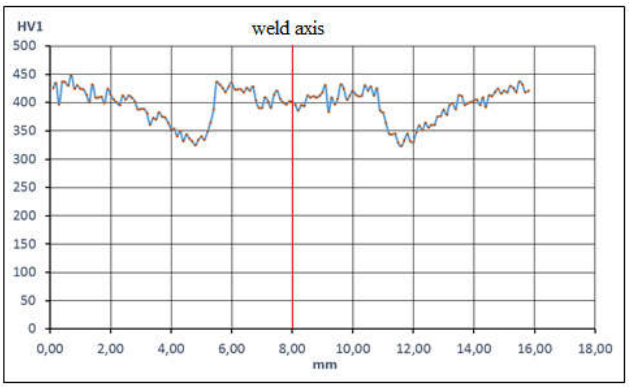

Figure 6. HV1 hardness of welded joints made of steel S1100.

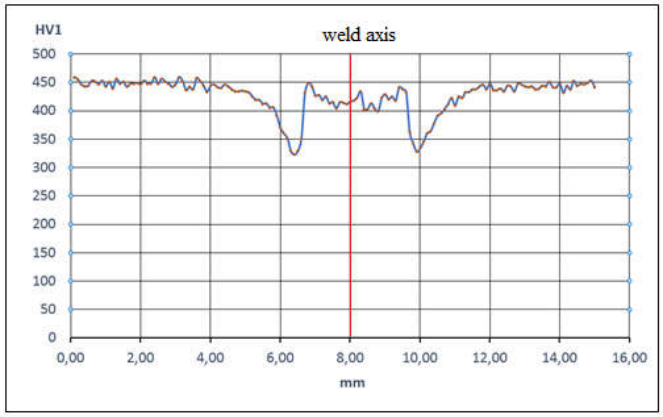

Figure 7. HV1 hardness of welded joints made of steel S1300.

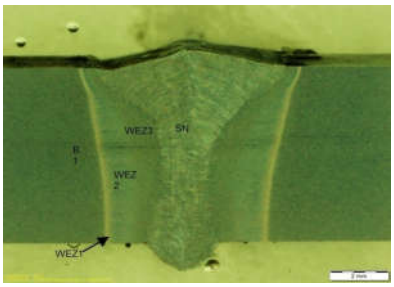

Macrostructure of the weldment.

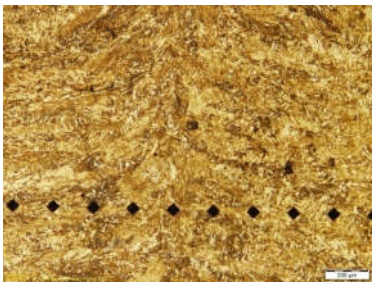

Axis of weld, coarse- grained martensite, HV 1 440-466.

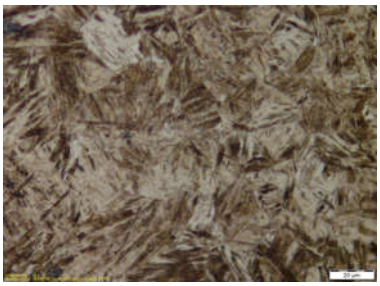

WEZ 3 hardeningstructure, HV1 478-492.

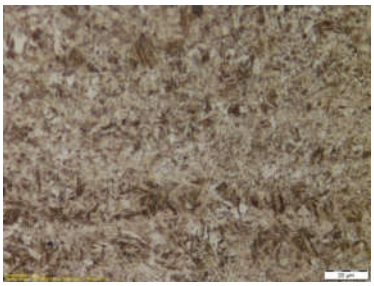

WEZ 2 Fine-grained martensit, HV1-500-520.

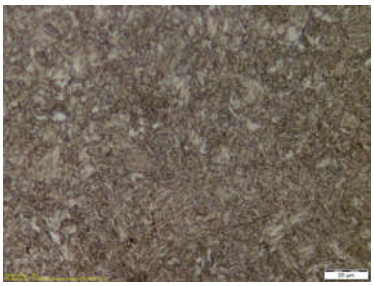

WEZ 1, fine-grained martensit and the areas with dense carbide precipitations, HV1-465.

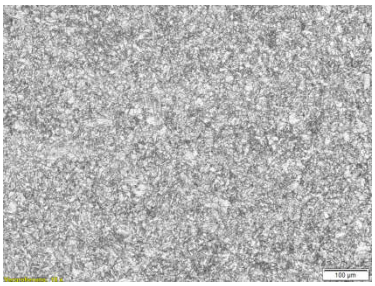

Base material tempered martensite and bainite, HV1-373-450.

Figure 8. Exemplary microstructure of welded joint of steel S1100.

Basically, the microstructure of the weld consists of a mixture of martensite and bainite. However, the microstructure of HAZ depends on the distance from the fusion line. It is composed of martensite near the fusion line and a mixture of bainite and ferrite in the vicinity of the base material. To assess the effect of cooling time $t_{8/5}$ on the microstructure, several samples of steel S1100 and S1300 were produced in bead on plate welds configuration. The welding parameters were calculated using the program WeldCalc based on the cooling time $t_{8/5}$. For $t_{8/5}$ 2, 8 and 15 seconds the microstructure and hardness were nearly the same, but microhardness in the weld seam by cooling time $t_{8/5}$ of 2 seconds had a higher dispersion than of 15 seconds.

5. Electron beam cutting

Most thermal cutting processes employ a concentrated gas jet directed onto the process zone to remove molten metal from the kerf figure 9a. Contrasting to conventional cutting processes, we were able to realize a cutting process that utilizes a local low vacuum underneath the process zone figure 9b.

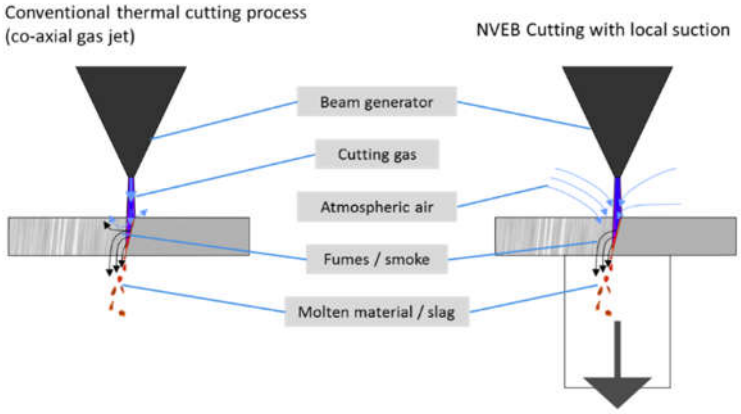

a) b)

Figure 9. Two different methods to remove molten material from the cutting kerf during thermal cutting.

This is realized providing an area with under-pressure or low-vacuum between 100 and 500 mbar using a sliding seal. The electron beam melts the material and due to the pressure gradient between both sides of the work-piece a strong gas flow is induced across the melting front, carrying molten and evaporated metal as well as smoke away from the kerf. This approach avoids high stagnation pressure in the kerf, which increases the beam power density and therefore achieves very high cutting speeds. The gas flow can interact precisely at the melt front and will force the molten metal downwards.

In contrast to a trailing gas jet, there is no dependence on the direction of the cut, so that curved contours can easily be realized. It is important to notice that this method requires no change to the beam generator or pressure stage system of the original NVEB welder. This means that the machine can be directly used for both processes - cutting and welding. To enable free choice of the cutting contour a sliding seal set-up has been developed, see figure 10. A pump taken from commercial vacuum clamping technology provides low pressure at the upper side of the work-piece. A simple silicone O-ring gasket provides enough sealing and the pressure regularly reaches 20-500 mbar depending on surface quality. Deflector plates and fine steel mesh filters as well as 10 m long metallic corrugated hose were used to protect the vacuum pump from hot metal droplets. The cutting head is adjustable in z-direction to adapt for different plates thicknesses. In addition to that, it is spring mounted to compensate for uneven plate surfaces. The bottom opening can be accessed to remove waste cutting material that accumulates in the lower arm of the cutting head.

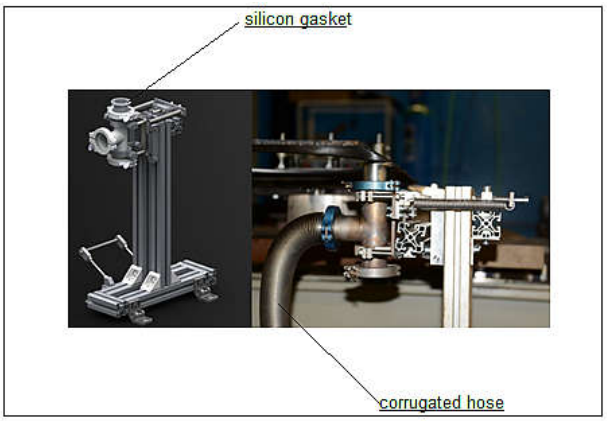

Figure 10. Working prototype for NVEB cutting with local suction used for the examinations enabling the processing of large plates [7].

The 5.3 mm plates of S1100 and S1300 were cut with a cutting speed up to 7 m/min., 70-90 mA beam current and working distance 2 mm. The cutting edges are smooth and show only minimal droplet formation. The resulting slope angle was 2.1˚, which corresponds to 2 of the 5 bevel levels in accordance with ISO 9013. The exemplary of the cutting edges are displayed in figure 11. Metallographic examinations showed a HAZ of 50-70 µm thickness exhibits fine-grained martensite structure caused by the cutting process (figure 12).

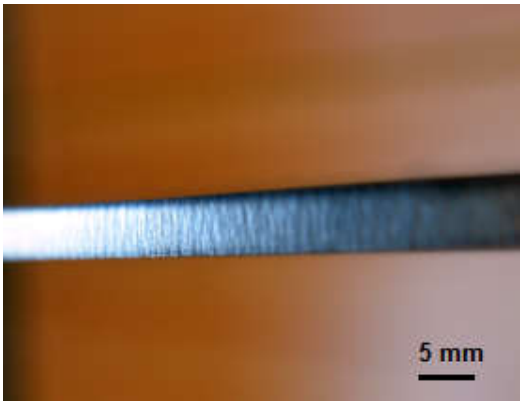

Figure 11. The cutting edge of 5.3 mm steel S1100.

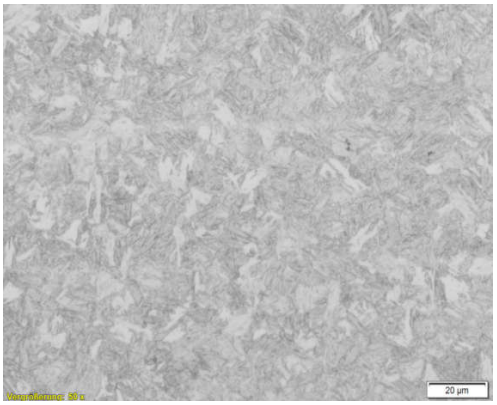

Figure 12. Microstructure of HAZ of cutting edge.

6. Process chain with one Single NVEB Machine

To assess the process chain of cutting and subsequent welding using the atmospheric electron beam, an exemplary task from industrial practice was reproduced in laboratory scale at IW as outlined in figure 13.

A 5.3 mm thick plate made of S1100QL steel was cut using NVEBC with local suction to create a 420 mm diameter hole. In a subsequent step, a functional component made of 5.2 mm thick S960QL steel was welded into the hole as a one pass butt joint using NVEBW with diam. 1.2 mm filler wire X70. These weld seams were subsequently characterized in multiple ways. In the first step of the process chain, the NVEB cutting technique was used to make circular cut-outs for flange connections. The cutting speed was 5 m/min and the beam current was 75 mA. The process duration for the cutting-out of a hole with a diameter of 420 mm was less than 16 s. These work-pieces were used without further processing for single-pass butt welds. Then the prepared billet was inserted into the hole and has been welded at 3 m/min with 100 mA beam current. Filler wire with a feed rate of 9.5 m/min was used. Weld face and root were flat and of good quality. The weld seams were analyzed using X-ray radiography. The X-ray radiographs showed no weld defects, in particular no pores or cracks. A

sample is given in figure 14. The work-piece has been cut into several specimens for metallographic examination and tensile testing.

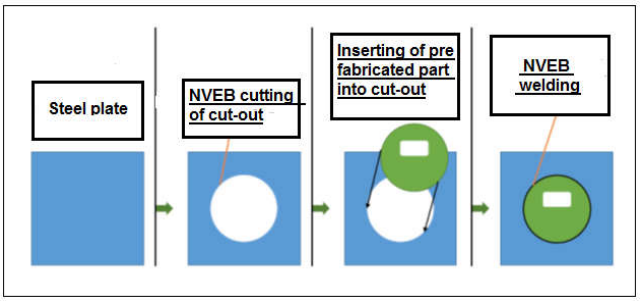

Figure 13. Flow diagram of the exemplary process chain using NVEB cutting and subsequent NVEB welding to insert functional element into a flat plate of high-strength steel.

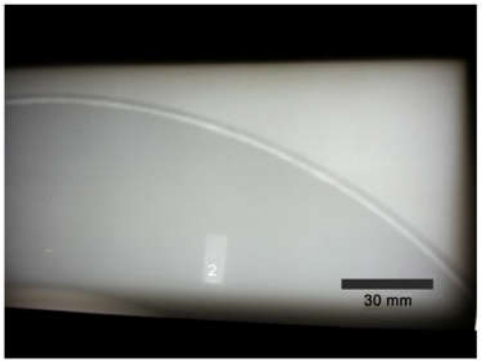

Figure 14. X-ray radiograph of a weld seam from an exemplary process chain of NVEBC and NVEBW [7].

The eight specimens according to DIN EN ISO 6892-1 and DIN 50125 were examined by tensile testing using a Zwick Z250 universal testing machine. They showed average ultimate tensile strength of 1077 MPa (±15 MPa). All specimens failed in the bulk material of the S960QL side.

7. Conclusions

Based on the metallographic examination and mechanical tests of the NVEB welded joints of steel S960QL, S1100 and S1300 the following conclusions can be formulated:

1. Welding of high strength quenched and tempered steels is possible with using NVEBW technology.
2. Fundamental differences in the microstructure between tested steels were not observed.
3. The weld seam consists of martensite. The microstructure of the HAZ depends on the distance from the fusion line and consists of martensite near the fusion line and of mixture of bainite and martensite in the vicinity of the base material.
4. Significant influence of cooling time $t_{8/5}$ up to 15 sec. on the microstructure of welded seam was not found.
5. In the case of welding of steel S960QL sufficient mechanical properties are obtained.
6. One single NVEB installation can be used for welding and cutting without changes on the construction.
7. Due to the high power density and the absence of a vacuum chamber, the electron beam in the atmosphere is a universal tool for various technological processes. Both, the NVEB welding process as well as the NVEB cutting process make use of these properties leading to highly productive and economic manufacturing of parts in mechanical engineering.

Acknowledgements

are made to Mr. Perndorfer, Director of Perndorfer Machienbau KG for his support of this work.

References

[1] Hamme U, Hauser J, Kern A and Schriever U 2000 *Stahlbau* **69** Heft 4
[2] Magej K and Jachym R 2017 *Buletyn Institutu Spawalnitctwa* (Poland) **2** pp 6-16
[3] Węglowski M, Zemanand M and Łomozik M 2013 *Physical Simulation of Weldability of Weldox 1300 Steel Materials Science Forum* (Trans Tech Publications: Switzerland) **762** pp

551-555
[4] Blacha S, Weglowski M S, Dymek S and Kopyscianski M 2017 *Arch. Metall. Mater* **62**(2) 627-634
[5] Murray N, Konya R, Beniyash A, Bach Fr-W and Hassel T 2012 *2nd International Electron Beam Welding Conference* (Aachen, Germany) DVS-Berichte 285 ISBN: 978-3-87155-299-1 DVS Media GmbH Düsseldorf
[6] Bach Fr-W, Beniyash A, Hassel T, Konya R, Murray N and Ruchay W Methodsand devices for thermal processing of workpieces with an electron beam and gas *Patent EP 2 322 309 B1*
[7] Hassel T, Murray N, Klimov G and Beniyash A 2016 *World Journal of Engineering and Technology* **4** 598-607
[8] Gerster P 2000 MAG-Schweißenhöhfester Feinkornstaähle im Fahrzeugkranbau, *Schweißen und Schneiden 2000 in Nürnberg* DVS Berichte Band 209 DVS Media GmbH Düsseldorf
[9] https://www.ssab.nl/support/calculators-and-tools
[10] Bach Fr-W, Beniyash A, Flade K, Szelagowski A, Versemann R and Zelt M 2003 *Nonvakuum Elektronenstrahlschweißen ein Hochleistungsverfahren zum Fügen von Magnesium und Aluminium-Legierungen Metall* **5**
[11] Data sheet SSAB 2017, S960, Strenx 1100, Strenx 1300